Chinese Chemical Letters 37 (2026) 111634

Contents lists available at ScienceDirect

Chinese Chemical Letters

journal homepage: www.elsevier.com/locate/cclet

Energy engineering and mechanical elasticity of molecular crystals *via* supramolecular salt strategy for flexible visible optical waveguide

Lizhi Wang[a,1], Chuanxin Wei[a,1], Xinyu Du[a], Yingying Zheng[a], Shuang Li[a], Ning Sun[a], Zhiqiang Zhuo[a], Ningning Yu[a], Yingru Lin[a], Zhiyang Sun[a], Jinyi Lin[a,c], Man Xu[b], Yongzheng Chang[b], Tianshi Qin[a], Zhoulu Wang[a], Xuehua Ding[a,*], Wei Huang[a,b]

[a] *State Key Laboratory of Flexible Electronics (LoFE) & Institute of Advanced Materials (IAM), School of Flexible Electronics (Future Technologies), Nanjing Tech University (NanjingTech), Nanjing 211816, China*
[b] *State Key Laboratory of Flexible Electronics (LoFE), School of Chemistry and Life Sciences, Nanjing University of Posts and Telecommunications, Nanjing 210023, China*
[c] *School of Chemistry and Chemical Engineering, Institute of Quantum and Sustainable Technology (IQST), Jiangsu University, Zhenjiang 212013, China*

ARTICLE INFO

Article history:
Received 24 April 2025
Revised 7 July 2025
Accepted 23 July 2025
Available online 25 July 2025

Keywords:
Supramolecular salt strategy
Flexible molecular crystals
Energy engineering
Optical property
Flexible visible optical waveguide

ABSTRACT

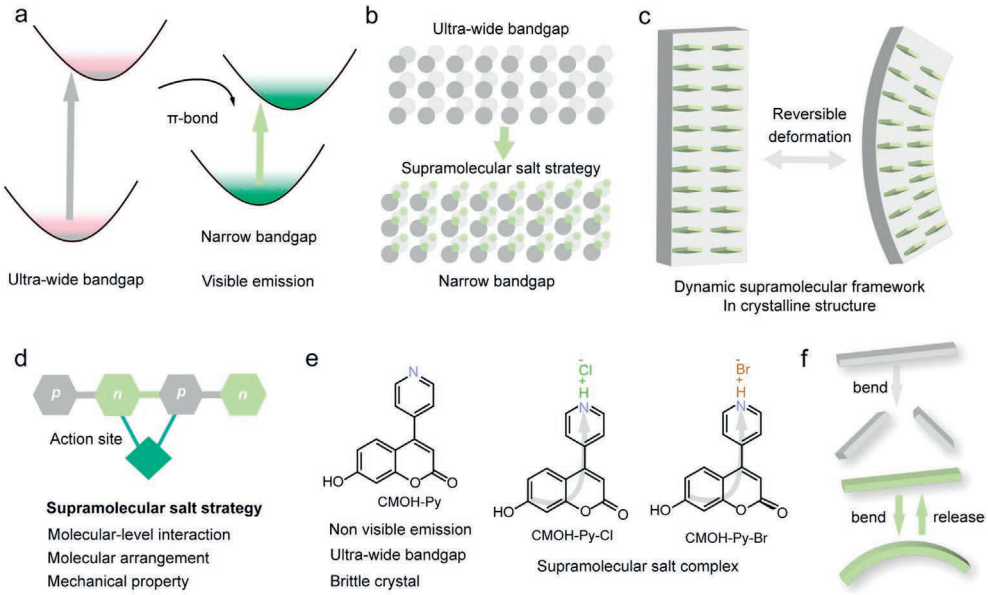
Improving the optoelectronic behavior and stress-deformation stability of conjugated materials is crucial for the realization of their potential applications in flexible optoelectronics. To tune the emission behavior and mechanical property of molecular crystals simultaneously *via* supramolecular salt strategy is rarely reported, which is very important to improve their photophysical behavior and softness for the fabrication of flexible light-emitting device. Herein, supramolecular salt approach has been successfully applied to synthesize two elastic organic fluorescent crystals (CMOH-Py-Cl and CMOH-Py-Br) derived from non-emissive and brittle pyridine-substituted coumarin derivative (CMOH-Py). Their elastic properties can be attributed to the prevalent presence of numerous weak interactions introduced by halogen atoms, which are beneficial to the absorption and release of mechanical energy. Furthermore, density functional theory (DFT) calculations demonstrated a narrowing of the HOMO–LUMO energy gaps from CMOH-Py to CMOH-Py-Cl/CMOH-Py-Br *via* supramolecular salt approach. Finally, the application of flexible crystal materials in the field of optical waveguides has been investigated. The transformation of crystals in terms of photophysical and mechanical properties, achieved by the supramolecular salt approach, offers novel insights into the design and construction of flexible crystalline materials, providing a new path for the development of next-generation smart materials.

© 2025 Published by Elsevier B.V. on behalf of Chinese Chemical Society and Institute of Materia Medica, Chinese Academy of Medical Sciences.

Emerging flexible optoelectronics have attracted increasing attention in both fundamental research and industrial products [1–6]. This emergent field offers nearly infinite possibilities for the application of artificial optoelectronic components, spanning from soft artificial intelligence and implantable bioelectronics to high-quality flexible optical communications, stretchable displays, and smart wearable devices [7–12]. The materials required for flexible optoelectronic devices should simultaneously possess high fluorescence quantum efficiency, maintain stable luminescence under bending deformation, and achieve synergistic optimization of mechanical strength and durability [1]. However, the complex interaction mechanisms of flexible molecular crystals, coupled with multiple technical challenges in their preparation processes, currently limit practical applications [6]. To precisely optimize the electronic structure and intrinsically mechanical property of conjugated materials are essential to potential applications in flexible optoelectronics (Schemes 1a-c) [13]. To date, supramolecular salt approach is an effective and universal strategy to not only tune the electronic structure, but also improve the intrinsic softness of organic conjugated materials (Schemes 1b and c). To be specific, the supramolecular salt strategy is a molecular design and assembly methodology grounded in supramolecular chemistry principles. It involves the organization of charged molecular units (*e.g.*, cations and anions) into ordered structures *via* non-covalent interactions, such as ionic bonds, hydrogen bonds, and π-π stacking, thereby enabling the regulation of physicochemical properties of materials [14–16]. On the one hand, compared to traditional blended processing, to tune the energy level and bandgap of organic conjugated molecules *via* supramolecular strategy at molec-

* Corresponding author.
E-mail address: iamxhding@njtech.edu.cn (X. Ding).
[1] These authors contribute equally to this work.

https://doi.org/10.1016/j.cclet.2025.111634
1001-8417/© 2025 Published by Elsevier B.V. on behalf of Chinese Chemical Society and Institute of Materia Medica, Chinese Academy of Medical Sciences.



Scheme 1. Supramolecular salt strategy of molecular crystal for flexible optoelectronics. (a) Energy engineering of conjugated materials *via* p-n molecular design. (b) Control the energy bandgap *via* supramolecular salt approach. (c) Reversible deformation of molecular crystal *via* dynamic supramolecular framework. (d) Supramolecular action site in heteroatomic conjugated molecules to tune their energy bandgap and improve deformation stability for the potential application in flexible optoelectronics. (e) Energy engineering and mechanical elasticity of pyridine-substituted coumarin derivatives (CMOH-Py) crystals *via* supramolecular salt strategy for flexible visible optical waveguide. (f) Diagram of brittle and weak visible emission CMOH-Py crystal, and green emission and flexible CMOH-Py-Br crystal.

ular level, is more efficient in optimizing the charge transport to the photophysics of excited states (Schemes 1b and d) [17]. On the other hand, to introduce the dynamic supramolecular networks *via* supramolecular assembly can establish the energy dissipation center to obtain excellent flexibility (Schemes 1c and d) [18]. However, to date, simultaneously tuning the intrinsic electronic structure and mechanical behavior of organic conjugated materials *via* a supramolecular salt strategy has been rarely reported. This approach is key to enhancing their photophysical behavior and deformation tolerance, which is crucial for flexible optoelectronic applications.

π-Conjugated molecules consisted of a series of aromatic units to present alternative single and double bonds with an excellent π-electron delocalization (Scheme 1a), closely associated with their bandgap and energy level, which allow for excellent optical and electrical properties [19–22]. Compared to amorphous states, molecular crystals display the long-range ordered structure, low defect density, and high optical transparency, which are extensively utilized in the field of organic optoelectronics such as optical waveguides [23,24], organic light-emitting diodes (OLEDs), and laser medium [25–27]. However, their non-flexibility and brittleness pose a significant challenge for practical applications in flexible optoelectronics. Excitingly, the appearance of bendable organic crystals, starting with the plastically bent crystal of 2-(methylthio)nicotinic acid reported by Reddy and co-workers in 2005, has overturned the conventional wisdom regarding the intrinsic fragility of molecular crystals [28]. Thenceforth, there has been a growing interest in exploring flexible molecular crystals with elasticity or plasticity, rapidly becoming an emerging research frontier in view of their potential application in flexible optoelectronic devices, mechanosensors, mechanical actuators, biomimetic robotics, and so forth [29–35]. Therefore, rational supramolecular designs are essential, and inevitably, the intermolecular interactions in crystals that govern the deformation-induced dynamic networks and complicated photophysical processing need to be taken into consideration [36–39].

Herein, we employ the supramolecular salt strategy to regulate the luminescent properties and intrinsic mechanical performance

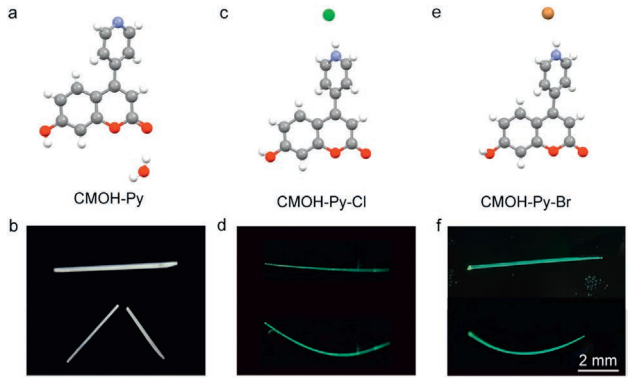


Fig. 1. Chemical structures and mechanical properties. (a, b) CMOH-Py structure and its brittle crystal. (c, d) CMOH-Py-Cl and (e, f) CMOH-Py-Br structures and corresponding elastic crystals under 365 nm UV light irradiation.

of molecular crystals, and conduct in-depth exploration of their applications in the field of flexible optical waveguides (Schemes 1e and f). As a result, significantly different to the non-emissive and brittle pyridine-substituted coumarin derivative (CMOH-Py), we have successfully obtained two elastic organic crystals (CMOH-Py-Cl and CMOH-Py-Br) (Scheme 1e). Interestingly, the introduction of acid component (HCl or HBr) enables both fluorescent emission and elastic flexibility of CMOH-Py crystal (Scheme 1f). Moreover, the crystals display a potential application in flexible optical waveguides, which exhibit low optical loss coefficients in both straight and bent configurations.

The chemical structures of coumarin derivatives CMOH-Py, CMOH-Py-Cl, and CMOH-Py-Br were depicted in Scheme 1 and Fig. 1, respectively. Acicular crystals of CMOH-Py, CMOH-Py-Cl and CMOH-Py-Br were all obtained by the slow evaporation of methanol solution at room temperature (CCDC: 2383523, 2327342 and 2327253; Experimental Section 1 in Supporting information). Multi-component CMOH-Py-Cl and CMOH-Py-Br crystals were prepared by co-crystallization of CMOH-Py with HCl and HBr acids, re-

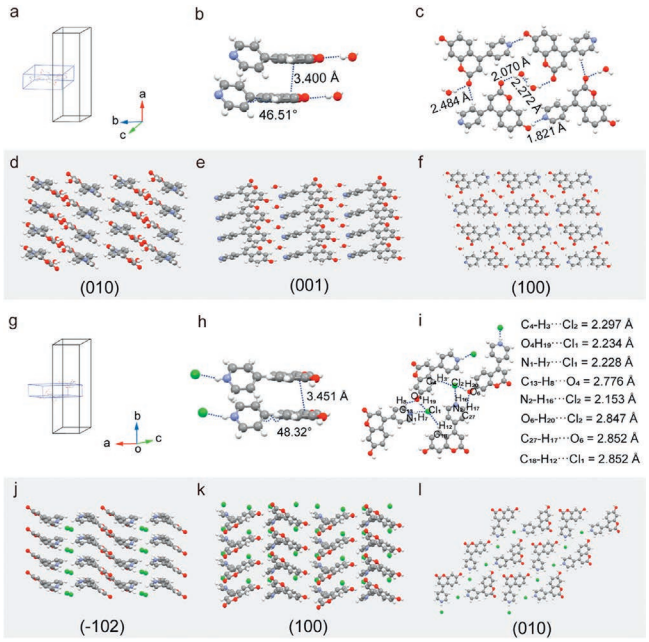


Fig. 2. Crystal structures of CMOH-Py and CMOH-Py-Cl. The crystal macroscopic model and molecular packing in CMOH-Py (a-f) and CMOH-Py-Cl (g-l).

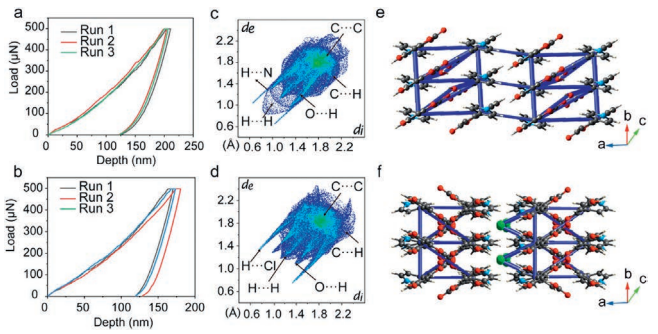


Fig. 3. Mechanical property and intermolecular interaction energy. Load-displacement curves of CMOH-Py (a) and CMOH-Py-Cl (b). The crystal Hirshfeld 2D fingerprint and Energy frameworks corresponding to total energy in CMOH-Py (c, e) and CMOH-Py-Cl (d, f).

spectively, in a 1:1 stoichiometric ratio. All the crystals had lengths of approximately 4–8 mm, widths ranging from tens to hundreds of micrometers, and thicknesses of tens of micrometers. CMOH-Py-Cl and CMOH-Py-Br showed similar crystal structures, with decomposition temperatures around 259 °C, demonstrating good thermal stability. However, the decomposition temperature of CMOH-Py crystals was much lower, at 147 °C, which was attributed to the presence of solvent water molecules within the crystal lattice (Fig. S1 in Supporting information). When fixing one end of the crystals and applying force to the other end, we observed that the CMOH-Py crystal was brittle and fractured rapidly (Figs. 1a and b). Interestingly, crystals of CMOH-Py-Cl and CMOH-Py-Br were capable of elastic bending. Upon the removal of external force, the bending crystals recovered to their original shape, and this deformation-recovery process can be repeated numerous times without the formation of any cracks (Figs. 1c-f). Scanning electron microscopy (SEM) confirmed that the crystal surface remained smooth after bending, with no cracks observed (Fig. S2 in Supporting information). Meanwhile, there was no visible emission observed for the CMOH-Py crystal under the 365 nm UV lamp excitation, due to its ultra-wide bandgap (>4.0 eV). Both CMOH-Py-Cl and CMOH-Py-Br crystals present a robust green emission, which is closely associated with their relative narrow bandgap (<3.0 eV) to realize the visible emission behavior (Scheme 1b).

The elasticity observed in various crystalline materials has been shown to originate from their crystal structures, as established in numerous studies [40,41]. Consequently, the crystal packings will be explored to compare the differences in different coumarin systems. Single-crystal X-ray diffraction (SCXRD) revealed that the compound CMOH-Py crystallizes in the triclinic system with the space group P-1. The unit cell parameters are $a = 3.8372(3)$ Å, $b = 11.0471(7)$ Å, $c = 13.8541(10)$ Å, $\alpha = 99.425(5)°$, $\beta = 96.219(5)°$, and $\gamma = 91.014(5)°$ (Table S1 in Supporting information). The largest face of the crystal corresponds to the (001) plane (Fig. 2a and Fig. S3 in Supporting information). In the CMOH-Py crystal, the molecules are stacked parallel to the a-axis *via* intermolecular $\pi\cdots\pi$ interactions with a distance of 3.400 Å (Figs. 2b and e). The molecular packing within CMOH-Py is stabilized by multiple hydrogen bonds, for instance, O−H···O (with distances of 2.070 Å and 2.272 Å, respectively), O−H···N (1.821 Å) and C−H···O (2.484 Å), all of which are oriented in the (100) planes (Figs. 2c and f). The presence of a substantial number of strong hydrogen bonds leads to fracturing of the crystal upon application of stress.

In contrast, multi-component CMOH-Py-Cl crystallizes in the monoclinic system with the space group *Pc*, having unit cell parameters of $a = 17.3829(8)$ Å, $b = 3.9696(2)$ Å, $c = 17.4512(8)$ Å, $\alpha = 90.00°$, $\beta = 100.233(3)°$, and $\gamma = 90.00°$ (Table S1 in Supporting information). The bending face of the crystal is the (100) plane (Fig. 2g and Fig. S3 in Supporting information). In the crystal structure of CMOH-Py-Cl, the molecules are tightly stacked along the b axis due to intermolecular $\pi\cdots\pi$ interactions, with a distance of 3.451 Å (Figs. 2h and k). Abundant intermolecular non-covalent interactions can be readily observed within the (010) planes, such as C−H···O (2.776, 2.852 Å, respectively), C−H···Cl (2.297, 2.852 Å, respectively), O−H···Cl (2.234, 2.847 Å, respectively) and N−H···Cl (2.228, 2.153 Å, respectively) (Fig. 2i). These weak interactions collectively form a "band-like structure" on the (010) plane (Fig. 2l). The presence of numerous weak interactions introduced by halogen atoms allows the CMOH-Py-Cl crystal to bend reversibly when the force was applied on the (100) face, which are beneficial to the absorption and release of mechanical energy and enhance the ability to resist fragmentation caused by external forces. The Hirshfeld 3D surface and 2D fingerprint analyses reveal that numerous weak intermolecular interactions (C/N/O−H···Cl) govern the molecular packing in CMOH-Py-Cl, unlike those strong hydrogen bonds (O−H···O/N) in CMOH-Py (Figs. 3c and d, Fig. S11 in Supporting information). In the crystal lattice, Cl-related interactions exert a significant influence on internal interactions, confirming that the introduction of halogen atoms contributes to enhancing the material's elasticity. Given that CMOH-Py-Br shows similar crystal structure and elastic property to CMOH-Py-Cl, its related information is provided Fig. S4 (Supporting information).

Subsequently, mechanical properties of the crystals were quantified using nanoindentation tests, with the load-displacement curves shown in Figs. 3a and b, and Table S2 (Supporting information). The average elastic modulus and hardness for the (001) plane of the CMOH-Py crystal are 9.02 GPa and 0.38 GPa, respectively. In the loading phase, a distinct pop-in event is noted, where the indenter experiences a sudden jump in displacement while the applied load remains steady. Research indicates that such pop-ins in molecular crystals occur when the applied force exceeds their resistive capacity, leading to the sudden yielding of the molecular layers beneath, which results in intermittent plastic deformation [42,43]. By contrast, the average elastic modulus and hardness for the (100) plane of the CMOH-Py-Cl crystal are 13.16 GPa and 0.48 GPa, respectively, which are higher than those of CMOH-Py, indicating that CMOH-Py-Cl possesses superior deformation recov-

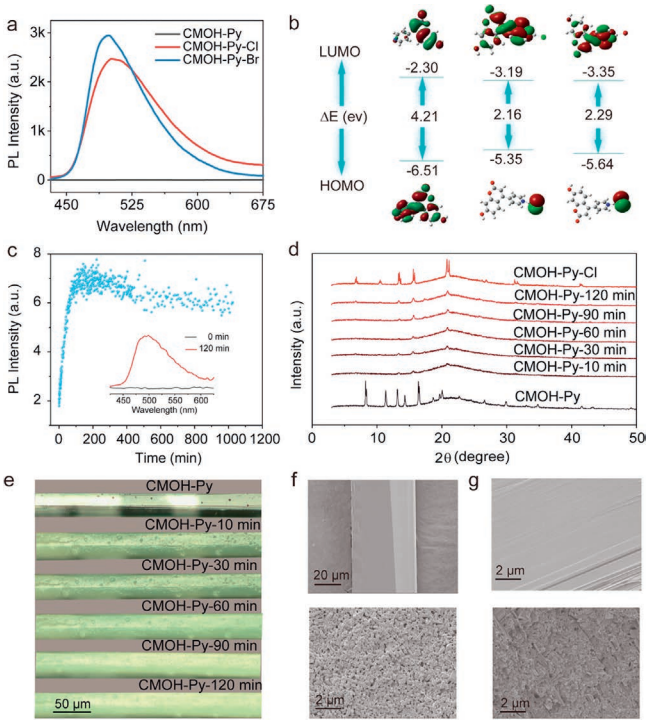


Fig. 4. (a) PL spectra of the CMOH-Py, CMOH-Py-Cl and CMOH-Py-Br crystal. (b) Molecular orbital amplitude plots and energy levels of the HOMOs and LUMOs of CMOH-Py, CMOH-Py-Cl and CMOH-Py-Br. (c) The PL intensity, (d) PXRD and (e) optical microscope image of the CMOH-Py crystal varies with time when exposed to HCl vapors. (f) SEM images of the CMOH-Py crystal surface and (g) its cross-section before and after exposure to HCl.

ery capability and better resistance to plastic deformation [44]. To further quantify intermolecular interactions, the energy framework analysis was carried out, which facilitates a more detailed understanding of the factors contributing to the crystal's flexibility. Due to the presence of numerous strong hydrogen bonds, the CMOH-Py crystal exhibits significant interaction energies on the (010) and (001) planes; once disrupted by external forces, it is not easy for these strong hydrogen bonds to reassemble reversibly, ultimately leading to crystal disintegration and fragmentation (Fig. 3e, Figs. S5 and S6 in Supporting information). In contrast, the crystal lattice in CMOH-Py-Cl presents weaker interlayer interaction energies on the (100) plane, while the intralayer interaction energies are more significant (Fig. 3f, Figs. S7 and S8 in Supporting information). The reduced interlayer binding energy allows for the presence of reversible molecular movements within a limited range, enabling the ability of elastic flexibility. Concurrently, the robust intralayer forces prevent the crystal from disintegrating under the influence of external forces.

When exploring the photoluminescent properties of coumarin systems, crystals of CMOH-Py show a non-fluorescent emission. However, upon cocrystallizing with volatile acids (HCl or HBr), the pyridine moiety in CMOH-Py will be protonated, resulting in multi-component crystals CMOH-Py-Cl or CMOH-Py-Br with green fluorescence emissions peaked at 500 nm or 490 nm, respectively (Fig. 4a and Fig. S15 in Supporting information). The lifetimes for CMOH-Py-Cl and CMOH-Py-Br were determined to be 2.94 ns and 2.87 ns, respectively, while the photoluminescence quantum efficiencies were calculated to be 12.54% and 15.67%, respectively (Fig. S16 in Supporting information). Compared with CMOH-Py, the pyridine moiety in CMOH-Py-Cl undergoes protonation to form a pyridinium ion, endowing an enhanced electron-withdrawing capability. This structural transformation leads to the establishment of a more pronounced D-π-A architecture, thereby reducing the bandgap of CMOH-Py-Cl and enabling its fluorescence emission. Density functional theory (DFT) calculations show that the energy gap of the highest occupied molecular orbital-lowest unoccupied molecular orbital (HOMO-LUMO) significantly narrows from CMOH-Py (>4.2 eV) to CMOH-Py-Cl/CMOH-Py-Br (<3.0 eV) (Fig. 4b). In this regard, the energy bandgap of heteroatomic conjugated molecules can be tuned *via* supramolecular strategy, which is useful to optimize their optical and electrical properties for the optoelectronic applications.

Intriguingly, the CMOH-Py crystal shows a response to volatile acid vapors, and then turns on a fluorescent switch rapidly. Take hydrochloric acid (HCl) as an example, upon exposure to HCl vapor, the CMOH-Py crystal undergoes an immediate transition from a non-fluorescent state to green fluorescence emission with a peak at 500 nm in accordance with the multi-component crystal CMOH-Py-Cl, further confirming the narrowing of their energy bandgap *via* supramolecular salt strategy. Subsequently, the fluorescence intensity increases gradually over time, reaching its maximum at approximately 120 min, and then maintains a constant level (Fig. 4c and Fig. S17 in Supporting information). The color of the CMOH-Py crystal gradually shifts from white to yellow (Fig. 4e). To investigate the changes in the crystal structure after the acid vapor treatment, powder X-ray diffraction (PXRD) experiments were conducted (Fig. 4d and Fig. S18 in Supporting information). Following exposure to HCl vapor for 10 min, weak diffraction peaks were detected at 2θ positions of 13.4°, 15.6°, and 20.9°. With the progression of time, the intensity of these diffraction peaks increases gradually, and no new diffraction peaks emerge. Comparison with the PXRD pattern of CMOH-Py-Cl revealed that the emerging diffraction peaks correspond to those characteristics of CMOH-Py-Cl, suggesting that exposure to hydrochloric acid vapor results in a gradual transformation of CMOH-Py to CMOH-Py-Cl, accompanied by relatively low crystallinity.

Nevertheless, it was observed that the acid treated crystal still maintained its original brittleness when we endeavored to manipulate it by fixing one end and then applying external force to the other. Subsequent scanning electron microscopy (SEM) analysis indicated that the surface integrity of the crystal exposed to hydrochloric acid vapor had been affected greatly, altering from smooth, unbroken crystal faces to numerous fragmented particles, each approximately 1 μm (Fig. 4f). The SEM image of the fractured cross-section indicated that the internal integrity of the crystal had been significantly compromised after exposure to HCl vapor. The previously smooth crystal planes were now altered into fragmented structures (Fig. 4g). This finding further corroborates that the inability of the post-fumigation crystal to be bent is attributable to the destruction of the integrity of crystal structure as a result of exposure to HCl vapor.

Organic crystals, due to their fewer defects and superior optical properties, are considered as candidate materials for optical waveguides [45–47]. By exciting different positions of the crystal with a 405 nm pulsed laser and collecting the emission spectra at the terminal, a series of distance-dependent emission spectra were obtained. It can be observed that the intensity of the emission spectra gradually decreases with the increase in the distance between the excitation end and the tip. By fitting the spectral data in the CMOH-Py-Cl crystal, the optical loss coefficient at the emission peak was calculated to be 0.02123 db/μm. When the CMOH-Py-Cl crystal was bent, similar phenomena were obtained and its optical loss coefficient was found to be 0.04494 db/μm, indicating the waveguiding capabilities were maintained even in the bent state. The results demonstrate that the CMOH-Py-Cl crystal exhibits a low optical loss coefficient in both straight and bent states, validating its potential as a flexible optoelectronic element (Fig. 5).

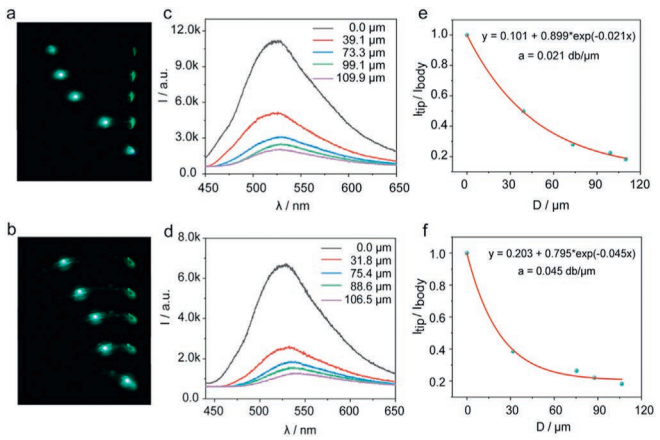


Fig. 5. Characterization of the optical waveguiding properties. Images of straight (a) and bent (b) CMOH-Py-Cl crystals excited at 405 nm at various positions. Fluorescence spectra collected from the tips of straight (c) and bent (d) CMOH-Py-Cl crystals with varying distances between the laser excitation point and the crystal tips. Decay of intensity with distance I_{tip}/I_{body} of CMOH-Py-Cl in straight (e) and bent (f) states.

In summary, a successful transformation of the molecular crystal from a non-emissive and brittle to fluorescent and elastic state was accomplished through supramolecular salt strategy for the flexible visible optical waveguide. The single crystal structure analysis and energy frameworks calculation manifested that the elastic properties in the two multi-component crystals (CMOH-Py-Cl and CMOH-Py-Br) could be attributed to the prevalence of numerous weak interactions introduced by halogen atoms. Moreover, the Hirshfeld surface analysis showed the halogen-related interactions had a significant impact on the internal crystal interactions, further demonstrating that the introduction of halogen atoms contributed to the elasticity of the crystal lattice. Additionally, DFT calculations indicated that bright green fluorescence emission in CMOH-Py-Cl/CMOH-Py-Br was ascribed to the narrowing of the HOMO–LUMO energy gaps. Interestingly, the CMOH-Py crystal can undergo a rapid fluorescence switch upon exposure to volatile acid vapors, which holds promise for the rapid acid detection. Furthermore, the CMOH-Py-Cl crystal exhibits a low optical loss coefficient, manifesting its potential application as a flexible waveguide. These results demonstrate that the supramolecular salt strategy has successfully worked on modulating the mechanical properties and photoluminescence characteristics of crystal, offering new insights into the design of next-generation smart materials.

Declaration of competing interest

There are no conflicts to declare.

CRediT authorship contribution statement

Lizhi Wang: Writing – original draft, Formal analysis, Data curation. **Chuanxin Wei:** Software, Methodology, Investigation. **Xinyu Du:** Resources, Formal analysis. **Yingying Zheng:** Visualization, Software, Conceptualization. **Shuang Li:** Validation, Software, Formal analysis. **Ning Sun:** Visualization, Validation, Software. **Zhiqiang Zhuo:** Resources, Conceptualization. **Ningning Yu:** Methodology, Investigation. **Yingru Lin:** Visualization, Validation, Software. **Zhiyang Sun:** Formal analysis, Conceptualization. **Jinyi Lin:** Validation, Funding acquisition, Conceptualization. **Man Xu:** Resources, Conceptualization. **Yongzheng Chang:** Resources, Methodology. **Tianshi Qin:** Visualization, Validation, Software. **Zhoulu Wang:** Investigation. **Xuehua Ding:** Writing – review & editing, Supervision, Project administration, Investigation. **Wei Huang:** Validation, Supervision.

Acknowledgments

This work is supported by the National Natural Science Foundation of China (Nos. 22205105, 61874053, 22075136), National Key Basic Research Program of China (No. 2020YFA0709900) and Jiangsu Provincial Postgraduate Scientific Research Innovation Program (No. KYCX24_1649).

Supplementary materials

Supplementary material associated with this article can be found, in the online version, at doi:10.1016/j.cclet.2025.111634.

References

[1] S. Chang, J.H. Koo, J. Yoo, et al., Chem. Rev. 124 (2024) 768–859.
[2] F.R. Fan, W. Tang, Z.L. Wang, Adv. Mater. 28 (2016) 4283–4305.
[3] J.H. Koo, D.C. Kim, H.J. Shim, et al., Adv. Func. Mater. 28 (2018) 1801834.
[4] B. Wang, A. Facchetti, Adv. Mater. 31 (2019) 1901408.
[5] Z. Wang, Z. Wang, D. Li, et al., Nature 626 (2024) 72–78.
[6] C. Wei, L. Li, Y. Zheng, et al., Chem. Soc. Rev. 53 (2024) 3687–3713.
[7] Y. Peng, J. Lu, X. Wang, et al., Nano Energy 94 (2022) 106945.
[8] P. Xue, C. Valenzuela, S. Ma, et al., Adv. Func. Mater. 33 (2023) 2214867.
[9] D. Won, J. Bang, S.H. Choi, et al., Chem. Rev. 123 (2023) 9982–10078.
[10] M.S. Cao, X.X. Wang, M. Zhang, et al., Adv. Mater. 32 (2020) 1907156.
[11] D. Zhong, C. Wu, Y. Jiang, et al., Nature 627 (2024) 313–320.
[12] Z. Zhuo, M. Ni, N. Yu, et al., Nat. Commun. 15 (2024) 7990.
[13] C.S. Boland, Y. Sun, D.G. Papageorgiou, Nano Lett. 24 (2024) 12722–12732.
[14] H. Wang, Q. Zhang, S. Chen, et al., ACS Appl. Mater. Interfaces 16 (2024) 56170–56180.
[15] G. Yang, X. Liu, L. Wang, et al., Angew. Chem. Int. Ed. 63 (2024) e202410454.
[16] S. Mondal, C.M. Reddy, S. Saha, Chem. Sci. 15 (2024) 3578–3587.
[17] J.R. Wu, G. Wu, D. Li, et al., Angew. Chem. Int. Ed. 62 (2023) e202218142.
[18] B. Liu, H. Liu, H. Zhang, et al., J. Phys. Chem. Lett. 11 (2020) 9178–9183.
[19] F.Y. Zhu, L.J. Mei, R. Tian, et al., Chem. Soc. Rev. 53 (2024) 3350–3383.
[20] A. Haque, K.M. Alenezi, M.S. Khan, et al., Chem. Soc. Rev. 52 (2023) 454–472.
[21] Y. Lin, L. Shen, J. Dai, et al., Adv. Mater. 29 (2017) 1604545.
[22] S.E. Root, S. Savagatrup, A.D. Printz, et al., Chem. Rev. 117 (2017) 6467–6499.
[23] C. Xing, B. Zhou, D. Yan, et al., CCS Chem. 5 (2023) 2866–2876.
[24] M. Dai, B. Zhou, D. Yan, Angew. Chem. Int. Ed. 64 (2025) e202505322.
[25] K. Wang, Z.Y. Lin, A. De, et al., Nature 633 (2024) 567–574.
[26] C. Wang, H. Dong, L. Jiang, et al., Chem. Soc. Rev. 47 (2018) 422–500.
[27] S. Zhao, J.X. Zhang, C.F. Xu, et al., Angew. Chem. Int. Ed. 63 (2024) e202412712.
[28] C.M. Reddy, R.C. Gundakaram, S. Basavoju, et al., Chem. Commun. 31 (2005) 3945–3947.
[29] L.C. An, X. Li, Z.G. Li, et al., Nat. Commun. 13 (2022) 6645.
[30] S. Das, A. Mondal, C.M. Reddy, Chem. Soc. Rev. 49 (2020) 8878–8896.
[31] X. Pan, L. Lan, L. Li, et al., Angew. Chem. Int. Ed. 63 (2024) e202320173.
[32] M. Rohullah, V.V. Pradeep, S. Singh, et al., Nat. Commun. 15 (2024) 4040.
[33] X. Ding, X. Du, L. Wang, et al., Matter 7 (2024) 2729–2731.
[34] F. Nie, D. Yan, Matter 6 (2023) 2558–2560.
[35] L. Lan, X. Pan, P. Commins, et al., CCS Chem. 7 (2025) 905–917.
[36] P. Marandi, D. Saini, K. Arora, et al., J. Am. Chem. Soc. 146 (2024) 26178–26186.
[37] S. Yousuf, J.M. Halabi, I. Tahir, et al., Angew. Chem. Int. Ed. 62 (2023) e202217329.
[38] J. Lin, J. Zhou, Z. Wang, et al., Angew. Chem. Int. Ed. 64 (2025) e202416856.
[39] S. Li, D. Yan, ACS Appl. Mater. Interfaces 10 (2018) 22703–22710.
[40] A.J. Thompson, B.S.K. Chong, E.P. Kenny, et al., Nat. Mater. 24 (2025) 356–360.
[41] A.J. Thompson, J.R. Price, J.C. McMurtrie, et al., Nat. Commun. 12 (2021) 5983.
[42] S. Varughese, M.S.R.N. Kiran, U. Ramamurty, et al., Angew. Chem. Int. Ed. 52 (2013) 2701–2712.
[43] M.S.R.N. Kiran, S. Varughese, C.M. Reddy, et al., Cryst. Growth Des. 10 (2010) 4650–4655.
[44] C. Wei, L. Bai, X. An, et al., Chem 8 (2022) 1427–1441.
[45] Y. Lin, S. Liu, D. Yan, Research 6 (2023) 0259.
[46] M. Dai, Z. Qi, D. Yan, Angew. Chem. Int. Ed. 64 (2025) e202420139.
[47] B. Tang, S. Tang, C. Qu, et al., CCS Chem. 5 (2023) 2348–2357.